CrystEngComm

RSC Publishing

PAPER

View Article Online
View Journal | View Issue

Coordination polymers of lanthanide complexes with benzene dicarboxylato ligands†

Cite this: *CrystEngComm*, 2013, **15**, 6340

Yu-Hui Luo,[a] Feng-Xia Yue,[a] Xiao-Yang Yu,[ab] Xin Chen*[c] and Hong Zhang*[a]

Received 27th February 2013,
Accepted 30th May 2013

DOI: 10.1039/c3ce40357b

www.rsc.org/crystengcomm

Three kinds of coordination polymers of lanthanide complexes with benzene dicarboxylato ligands, $[Ln(L^1)_{1.5}(H_2O)_2]\cdot H_2O$ (H_2L^1 = 2,5-dibenzoylterephthalic acid; Ln = Pr (**1**), Nd (**2**), Sm (**3**), Eu (**4**), Gd (**5**), Tb (**6**), Dy (**7**)), $[Ln(L^2)(phen)(OH)]$ (H_2L^2 = 4,6-dibenzoylisophthalic acid; phen = 1,10-phenanthroline; Ln = Sm (**8**), Eu (**9**), Tb (**10**), Dy (**11**), Er (**12**), Yb (**13**)) and $[Ln(L^1)_{0.5}(L^2)(H_2O)_2]$ (Ln = Er (**14**), Ho (**15**)), were synthesized under hydrothermal conditions. They were characterized by elemental analysis, IR spectroscopy and thermogravimetric analysis. Their solid-state structures were determined by single-crystal X-ray diffraction. Complexes **1–7** are isostructural, each featuring the L^1 connected dinuclear unit of $Ln_2O_2(CO_2)_6$ to produce a 6-connected 3D network with $(4^{12}\cdot6^3)$ topology. Isostructural complexes **8–13** possess 2D layer structures consisting of left- and right-handed helical chains that are further assembled into 3D supramolecular architectures through C–H···O, C–H···π and π···π interactions. Complexes **14** and **15** display 2D layer structures, and are further linked into 3D supramolecular architectures through C–H···O and π···π interactions. The luminescence properties of **3**, **4** and **6–11** were investigated.

Introduction

The design and syntheses of lanthanide–organic framework materials are attracting increasing attention, due to their often fascinating structures[1,2] and potentially useful applications associated with their unique luminescence[3–7] and magnetic properties,[8–10] as well as the Lewis acidity of the lanthanide ions.[11–13] In such designs, the use of aromatic ligands is common as they are excellent in sensitizing the lanthanide luminescence by the well-known ''antenna effect'', in which the ligands are first excited, followed by energy transfer from the ligand's singlet excited states to their triplet excited states (*i.e.* intersystem crossing), and then to the emissive states of the lanthanide ion.[6,14–17] Up to now, lanthanide–organic frameworks with a number of aromatic carboxylate ligands such as 1,3/1,4-benzenedicarboxylate[18–22] as well as modified 1,3/1,4-benzenedicarboxylate are known.[23–26] However, less effort has been paid to benzoyl substituted 1,3/1,4-benzenedicarboxylate, which can form versatile coordination structures. Firstly, carboxylate groups on the molecules can be completely deprotonated to form versatile coordination models. Secondly, the benzoyl on the ortho position of carboxylate group can also coordinate to metal ions with the carbonyl oxygen atom. Further more, the benzoyl can form C/O–H···O, C/O–H···π and π···π interactions as steering forces on the control of molecular self-assembly. We have recently reported four isomorphous lanthanide complexes with 4,6-bis(4-methylbenzoyl)isophthalate and 2,5-bis(4-methylbenzoyl)terephthalate as ligands, and have also studied their luminescence properties.[27] We have reported a rare 3D chiral framework constructed from left-handed helices and right-handed double helices with 4,6-dibenzoylisophthalic acid.[28] These results indicate that benzoyl substituted 1,3/1,4-benzenedicarboxylate is an excellent ligand in the self-assembly of coordination polymers. As an extension of our work, here we report the syntheses and characterization of fifteen new lanthanide complexes based on bulky benzoyl substituted aromatic dicarboxylic acids, namely, 2,5-dibenzoylterephthalic acid (H_2L^1) and 4,6-dibenzoylisophthalic acid (H_2L^2).

The fifteen new complexes, $[Ln(L^1)_{1.5}(H_2O)_2]\cdot H_2O$ (H_2L^1 = 2,5-dibenzoylterephthalic acid; Ln = Pr (**1**), Nd (**2**), Sm (**3**), Eu (**4**), Gd (**5**), Tb (**6**), Dy (**7**)), $[Ln(L^2)(phen)(OH)]$ (H_2L^2 = 4,6-dibenzoylisophthalic acid; phen = 1,10-phenanthroline; Ln = Sm (**8**), Eu (**9**), Tb (**10**), Dy (**11**), Er (**12**), Yb (**13**)) and $[Ln(L^1)_{0.5}(L^2)(H_2O)_2]$ (Ln = Er (**14**), Ho (**15**)), were all synthesized under hydrothermal conditions. Each kind of structure and the effects of benzoyl are discussed. Additionally, the luminescence properties of **3**, **4** and **6–11** were investigated.

[a]*Department of Chemistry, Institute of Polyoxometalate Chemistry, Northeast Normal University, Changchun, Jilin 130024, P. R. China. E-mail: zhangh@nenu.edu.cn*

[b]*Jilin Institute of Chemical Technology, College of Chemical and Pharmaceutical Engineering, Jilin City, Jilin, 132022, P. R. China*

[c]*School of Pharmaceutical & Life Sciences, Changzhou University, Changzhou, Jiangsu, 213164, P. R. China. E-mail: xinchen@cczu.edu.cn*

† Electronic supplementary information (ESI) available. CCDC 890964–890974 and 936978. For ESI and crystallographic data in CIF or other electronic format see DOI: 10.1039/c3ce40357b

Experimental

Materials and physical measurements

All the chemicals were purchased commercially and used as received without further purification. H_2L^1 and H_2L^2 were synthesized according to the literature procedures.[29] The FT-IR spectra were recorded using KBr pellets in the range of 4000–400 cm^{-1} on a Mattson Alpha-Centauri spectrometer. Elemental analyses for C, H and N were performed on a Perkin-Elmer 2400 Elemental Analyzer. Powder X-ray diffraction (PXRD) patterns were collected on a Rigaku D/Max 2000 X-ray diffractometer with graphite monochromatized Cu Kα radiation (λ = 1.5418 Å) and 2θ ranging from 5 to 50° with an increment of 0.02° and a scanning rate of 5° min^{-1}. Thermogravimetric analyses (TGA) were performed on a Perkin-Elmer Thermal Analyzer under an N_2 atmosphere at a heating rate of 5 °C min^{-1}. The luminescence studies were performed on a FLS920 Edinburgh Luminescence Spectrometer with a light source of a Xenon lamp. The wavelengths for the photoexcitation of each compound were set the maximum of the excitation spectra.

Preparation

Synthesis of $Pr(L^1)_{1.5}(H_2O)_2{\cdot}H_2O$ (1). The pH of the mixture of $Pr(NO_3)_3{\cdot}6H_2O$ (43.5 mg, 0.1 mmol), H_2L^1 (56.1 mg, 0.15 mmol) and 15 mL of H_2O was adjusted to about 4.5 with NaOH (aq. 0.1 M). The resulting mixture was sealed in a 23 mL Teflon-lined stainless steel container, and then heated at 160 °C for 3 d. Then the reaction system was cooled to room temperature at the rate of 3 °C h^{-1}. The product was isolated as light-green block crystals in 62% yield based on Pr. Elemental anal. calcd for $C_{33}H_{24}PrO_{12}$ (753.43): C, 52.61; H, 3.21%. Found: C, 52.69; H, 3.24%. IR bands (KBr pellet, cm^{-1}): 3445 (m), 3057 (w), 1668 (s), 1637 (m), 1595 (s), 1567 (m), 1479 (m), 1446 (m), 1397 (s), 1339 (m), 1253 (m), 1178 (w), 1144 (w), 1041 (w), 1021 (w), 953 (w), 926 (m), 893 (w), 806 (m), 767 (m), 693 (w), 624 (w), 524 (m), 491 (m). Complexes **2–7** were synthesized analogously but using different starting lanthanide salts (ESI†).

Synthesis of $Tb(L^2)(phen)(OH)$ (10). The pH of an aqueous solution containing $Tb(NO_3)_3{\cdot}6H_2O$ (45.3 mg, 0.1 mmol), H_2L^2 (37.4 mg, 0.1 mmol), and 1,10-phen (19.8 mg, 0.1 mmol) in 15 mL of H_2O was adjusted to about 5.0 with 0.1 M NaOH. The resulting mixture was sealed in a 23 mL Teflon-lined stainless steel container, and then heated at 160 °C for 3 d. Upon cooling to room temperature at the rate of 3 °C h^{-1}, the product was isolated as colorless prismatic crystals in 52% yield based on Tb. Elemental anal. calcd for $C_{34}H_{21}TbN_2O_7$ (728.46): C, 56.06; H, 2.91; N, 3.85%. Found: C, 56.01; H, 2.88; N, 3.84%. IR bands (KBr pellet, cm^{-1}): 3442 (s), 3059 (w), 1668 (s), 1587 (s), 1550 (m), 1517 (w), 1483 (w), 1394 (s), 1312 (w), 1254 (m), 1177 (w), 1139 (w), 1101 (w), 1042 (w), 921 (w), 892 (w), 775 (w), 724 (m), 609 (w), 498 (w), 426 (w). Complexes **8–9** and **11–13** were prepared in a similar way with different lanthanide starting materials (ESI†).

Synthesis of $Ho(L^1)_{0.5}(L^2)(H_2O)_2$ (15). The pH of an aqueous solution containing $Ho(NO_3)_3{\cdot}5H_2O$ (44.1 mg, 0.1 mmol), H_2L^1 (37.4 mg, 0.1 mmol) and H_2L^2 (37.4 mg, 0.1 mmol) in 15 mL of H_2O was adjusted to about 4.5 with 0.1 M NaOH. The resulting mixture was sealed in a 23 mL Teflon-lined stainless steel container, and then heated at 160 °C for 3 d. Upon cooling to room temperature at the rate of 3 °C h^{-1}, the product was isolated as colorless block crystals in 58% yield based on Ho. Elemental anal. calcd for $C_{33}H_{22}HoO_{11}$ (759.44): C, 52.19; H, 2.92%. Found: C, 52.23; H, 2.87%. IR bands (KBr pellet, cm^{-1}): 3442 (s), 3058 (w), 1655 (s), 1540 (m), 1480 (w), 1447 (w), 1403 (m), 1340 (w), 1313 (w), 1257 (m), 1179 (w), 1073 (w), 1043 (w), 1021 (w), 951 (w), 928 (w), 894 (w), 807 (w), 767 (w), 690 (w), 525 (w), 494 (w). Complex **14** was prepared similarly (ESI†).

X-Ray crystallography

Single crystals were glued to a fiberglass for X-ray diffraction data collection. Data sets of **1**, **3**, **10**, **12**, **13** and **14** were collected on Rigaku Mercury CCD diffractometer, those of **2**, **4**, **6**, **11** and **15** were collected on an Oxford Diffraction Gemini R Ultra diffractometer, and that of **5** was collected on a Bruker Smart Apex CCD diffractometer, using a graphite monochromated Mo Kα radiation (λ = 0.71073 Å) at 293 K. The intensity data sets of **1**, **3**, **10**, **12**, **13** and **14** were collected with the ω scan technique and corrected for Lp effects. Absorption corrections of **2**, **4**, **6**, **11** and **15** were applied using multi-scan technique. Absorption correction of **5** was applied by using SADABS. The structures were solved by the direct method followed by the difference Fourier method and refined by full-matrix least-squares on F^2 using the SHELXS-97 package.[30] All non-hydrogen atoms were refined anisotropically. The restraint command "ISOR" was used to restrain atoms C9, C10, C30, C31 in **1**; C9, C10, C20, C21 in **2**, **3** and **4**; C9, C10, C30, C31, C32 in **5**; C19, C20, C21, C30, C31, C32 in **6**; C9, C10, C20, C30, C31 in **10**; C13, C14, C19, C20, C21, C30, C31 in **11**; C13, C19, C20, C27, C28 in **12**; and C11, C12, C13, C18, C19, C20, C27, C28 in **13**. Hydrogen atoms were added according to the theoretical models. The hydrogen atoms of the OH group were decided by charge balance and cannot be located from difference Fourier maps. Selected crystal data and data collection and refinement parameters are listed in

Table 1 Crystal data and structure refinement parameters for **1**, **10** and **15**

Complexes	**1**-Pr	**10**-Tb	**15**-Ho
Formula	$C_{33}H_{24}PrO_{12}$	$C_{34}H_{21}TbN_2O_7$	$C_{33}H_{22}HoO_{11}$
Formula weight	753.43	728.46	759.44
Space group	$P\bar{1}$	$P2_1/c$	$P\bar{1}$
a/Å	10.442(2)	11.9617(6)	10.1326(5)
b/Å	11.545(2)	12.6849(5)	10.1834(4)
c/Å	14.071(3)	19.6998(10)	15.5265(8)
α (°)	102.208(2)	90	96.308(4)
β (°)	110.931(1)	107.951(3)	97.128(4)
γ (°)	100.536(1)	90	113.890(4)
V/Å^3	1485.2(5)	2843.6(2)	1430.69(12)
Z	2	4	2
μ/mm^{-1}	1.708	2.542	2.831
F(000)	754	1440	750
R_{int}	0.0184	0.0301	0.0427
Goodness of fit on F^2	0.987	1.074	0.995
$R_1{}^a$, $wR_2{}^b$ [$I > 2\sigma(I)$]	0.0234, 0.0613	0.0352, 0.0902	0.0452, 0.0624
R_1, $wR_2{}^b$ (all data)	0.0261, 0.0613	0.0445, 0.1212	0.0589, 0.0687

^{a} $R_1 = \Sigma||F_o| - |F_c||/\Sigma|F_o|$. ^{b} $wR_2 = \Sigma[w(F_o{}^2 - F_c{}^2)^2]/\Sigma[w(F_o{}^2)^2]^{1/2}$.

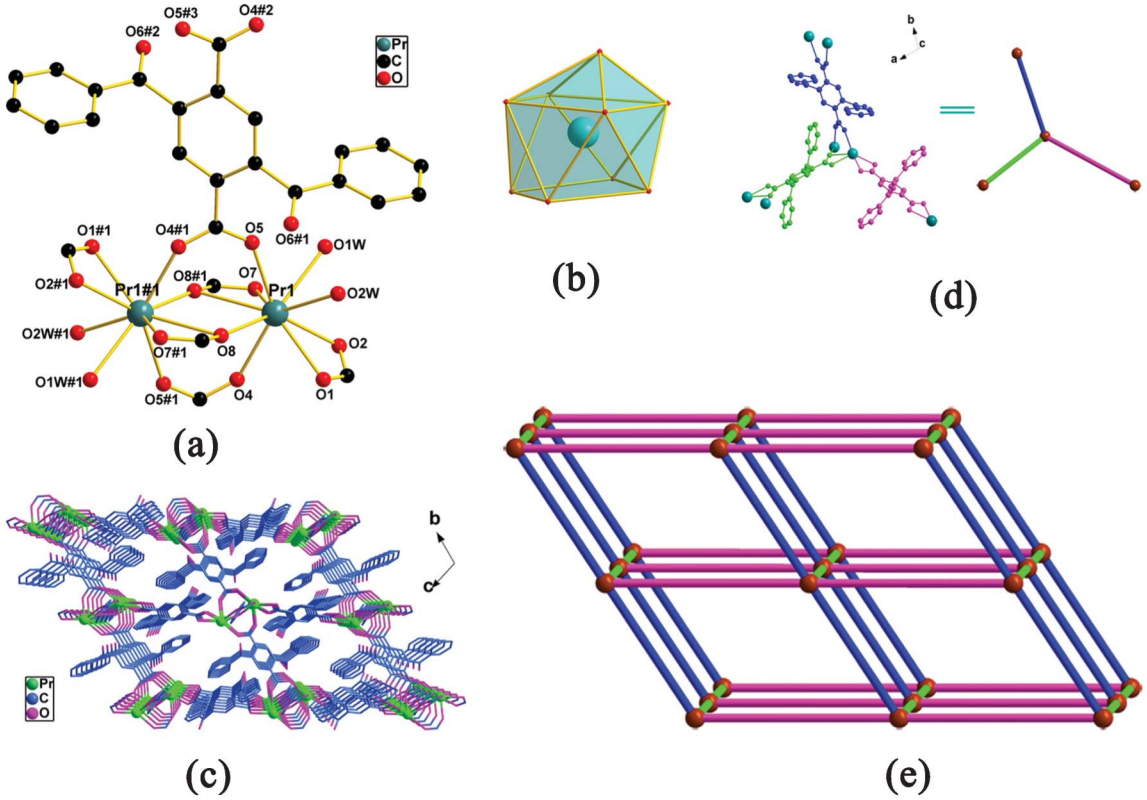

Fig. 1 (a) Coordination environment of the Pr(III) ion in **1** (symmetry codes: #1: $-x+1, -y+1, -z+1$; #2: $x, y-1, z$; #3: $-x+1, -y, -z+1$). (b) The slightly distorted monocapped square-antiprism geometry of the Pr(III) ion. (c) View of the 3D framework of **1**. (d) The binuclear $Pr_2O_2(CO_2)_6$ subunits are defined as 6-connected nodes, and the L^1 ligands are simplified to be linear connectors. (e) The 3D network with the default **pcu** net ($4^{12}\,6^3$).

Table 1 and the remaining are listed in ESI,† Table S1. The selected bond lengths and bond angles of **1–6** and **10–15** are listed in ESI,† Table S7. CCDC reference numbers are as follows: 890964 (**1**), 890967 (**2**), 890968 (**3**), 890969 (**4**), 890970 (**5**), 936978 (**6**), 890971 (**10**), 890972 (**11**), 890973 (**12**), 890974 (**13**), 890965 (**14**) and 890966 (**15**).

Results and discussion

Crystal structure description

Crystal structures of 1–7. Single-crystal X-ray diffraction and Powder X-ray diffraction analyses reveal that complexes **1–7** are isostructural. Therefore, only the crystal structure of **1** is discussed in detail. Complex **1** crystallizes in the triclinic space group $P\bar{1}$. Its asymmetric unit contains one crystallographically independent Pr(III) ion, one and a half L^1 anions, two coordinated and one lattice water molecules. As shown in Fig. 1a, atom Pr1 is nonacoordinate by seven carboxylate oxygen atoms from five L^1 ligands (O1, O2, O4, O5, O7, O8, O8#1 (#1: $-x+1, -y+1, -z+1$)) and two aqua ligands (O1W, O2W), forming a slightly distorted monocapped square-antiprism geometry (Fig. 1b). The Pr–O bond lengths range from 2.440(2) to 2.710(2) Å (the average length is 2.5262 Å), and O–Pr–O bond angles are in the range 49.84(8)–148.06(8)°, which are comparable to those reported earlier for other Pr(III)–O complexes.[31,32] As listed in Table S2 (ESI†), it can be seen that the Ln–O bond lengths (Ln = Pr (**1**), Nd (**2**), Sm (**3**), Eu (**4**), Gd (**5**), Tb (**6**)) decrease slightly as the atomic numbers of Ln increase, consistent with lanthanide contraction. In the polymeric structure of **1**, all carboxylic groups are deprotonated and L^1 ligands display three types of bridging modes: μ_4-(η^1:η^2)-(η^1:η^2) (**a**), μ_2-(η^1:η^1)-(η^1:η^1) (**b**) and μ_4-(η^1:η^1)-(η^1:η^1) (**c**) (Scheme 1a–1c). Four carboxylate groups from four L^1 ligands act as bidentate (*syn–syn* mode) and chelating–

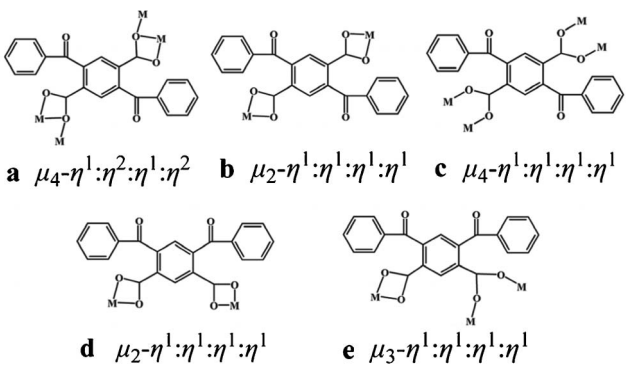

Scheme 1 Three coordination modes (**a**–**c**) of L^1 and two coordination modes (**d** and **e**) of L^2.

bridging bidentate bridges for two adjacent crystallographically equivalent Pr(III) ions to generate an irregular paddle-wheel-like $Pr_2O_2(CO_2)_6$ subunit with a Pr···Pr distance of 4.0610(8) Å. The Ln···Ln (Ln = Pr (**1**), Nd (**2**), Sm (**3**), Eu (**4**), Gd (**5**), Tb (**6**)) distances are listed in Table S2, ESI.† The modes **a**, **b** and **c** of the L^1 ligands bridge the adjacent $Pr_2O_2(CO_2)_6$ subunits extending in three different directions to form a 3D architecture (Fig. 1c and 1d). Moreover, significant intramolecular C/O–H···O (O1W–H1WA···O3W; O2W–H2WA···O9; O3W–H3WA···O2; O3W–H3WB···O7; C14–H14···O3; C25–H25···O2W and C30–H30···O3W) hydrogen-bonding interactions and C–H···π (C31–H31 > Cg(2) Cg(2): C6 > C7 > C8 > C9 > C10 > C11) interactions help to stabilize the structure. (Tables S3 and S4 in ESI†).

From a topological perspective, if the binuclear $Pr_2O_2(CO_2)_6$ subunits are defined as 6-connected nodes, and the L^1 ligands are simplified as linear connectors as shown in Fig. 1d, the structure of **1** can be described as a six-connected 3D network with the default **pcu** net ($4^{12}\cdot6^3$).

Crystal structures of 8–13. According to the single-crystal X-ray diffraction and Powder X-ray diffraction, complexes **8–13** are isostructural and crystallize in monoclinic space group $P2_1/c$. As a representative, the crystal structure of **10** is described in detail. The asymmetric unit of **10** consists of one crystallographically independent Tb(III) ion, one L^2 anion, one 1,10-phen and one μ_2-OH group. As shown in Fig. 2a, the Tb(III) center is octacoordinated by four carboxylate oxygen atoms (O1, O2, O4#2, O5#2 (#2: $-x+1, y+1/2, -z+3/2$)) from two L^2 ligands, two oxygen atoms (O7, O7#1 (#1: $-x+1, -y+1, -z+1$)) from two different μ_2-OH groups and two nitrogen atoms (N1 and N2) from one 1,10-phen forming a distorted dodecahedral geometry (Fig. 2b). The Tb–O bond lengths range from 2.270(3) to 2.517(4) Å (average 2.3858 Å), and the Tb–N bond lengths are 2.560(4) and 2.574(4) Å, respectively, which are comparable to those reported earlier of other Tb(III) complexes.[33] As listed in Table S2 (ESI†), it can be seen that the Ln–O and Ln–N bond lengths (Ln = Tb (**10**), Dy (**11**), Er (**12**), Yb (**13**)) decrease slightly as the atomic numbers of Ln increase, consistent with lanthanide contraction. In **10**, L^2 ligands exhibit the μ_2-(η^1:η^1)-(η^1:η^1) (**d**) (Scheme 1d) mode and bridge the Tb(III) ions to form 1D left- and right-handed helical $[TbL^2]_n$ chains running along the *b* axis with a pitch of 12.685 Å. The alternately arranged left- and right-handed helical chains are bridged by μ_2-OH groups, leading to an achiral 2D layer in the *bc* plane (Fig. S1, ESI†). As shown in Fig. 3a, six Tb(III) atoms are connected by four L^2 ligands and two μ_2-OH groups to form a parallelogram unit. Two 1,10-phen ligands, chelating to two Tb(III) centers, respectively, fill in the parallelogram unit and are parallel to each other with a face-to-face distance of 3.490 Å (Cg(6) > Cg(6), Cg(6): C(26) > C(27) > C(28) > C(29) > C(30) > C(31)), indicating π···π stacking interactions. From a topological perspective, Tb(III) atoms function as 3-connected nodes, while μ_2-OH groups and L^2 ligands can be viewed as linear connectors. Thus, the overall framework can be described as a 3-connected 2D network with (6^3) topology (Fig. 3b). Notably, the adjacent 2D layers are linked together into a 3D supramolecular architecture through C–H···O hydrogen bonds (C21–H21···O3) (Fig. 3c), C–H···π (C18–H18 > Cg(4) Cg(4): C6 > C7 > C8 > C9 > C10 > C11) and π···π (Cg(5) > Cg(5) Cg(5): C17 > C18 > C19 > C20 > C21 > C22) interactions (Fig. S2, ESI†). The detailed parameters of C–H···O hydrogen bonds and C–H···π and π···π interactions are listed in the ESI,† Tables S2–S5.

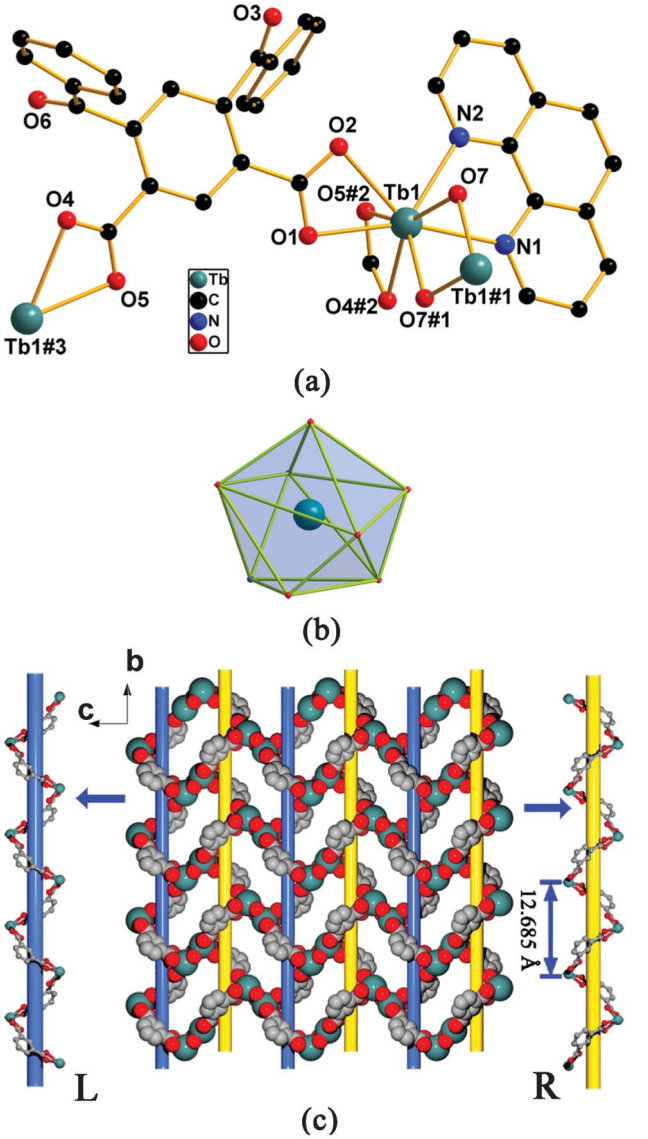

Fig. 2 (a) The coordination environment of the Tb(III) ion in **10** (symmetry codes: #1: $-x+1, -y+1, -z+1$; #2: $-x+1, y+1/2, -z+3/2$; #3: $-x+1, y-1/2, -z+3/2$). (b) The distorted dodecahedral geometry of the Tb(III) ion. (c) View of the left- and right-handed helical chains (shown in ball-and-stick representative) and achiral 2D layer (shown in space-filling representative). All H atoms are omitted for clarity.

Crystal structures of 14–15. The two isostructural complexes **14–15** crystallize in the triclinic space group $P\bar{1}$ and exhibit 2D layer structures. Thus only the structure of **15** is described in detail. The asymmetric unit of **15** consists of one crystallographically independent Ho(III) ion, half of an L^1 anion, one L^2 anion and two water molecules. As shown in Fig. 4a, Ho(III) center is octacoordinated by two carboxylate oxygen atoms (O7#1, O8 (#1: $-x+1, -y+1, -z+1$)) from one L^1 ligand, four carboxylate oxygen atoms (O1#1, O2, O3, O4) from two L^2

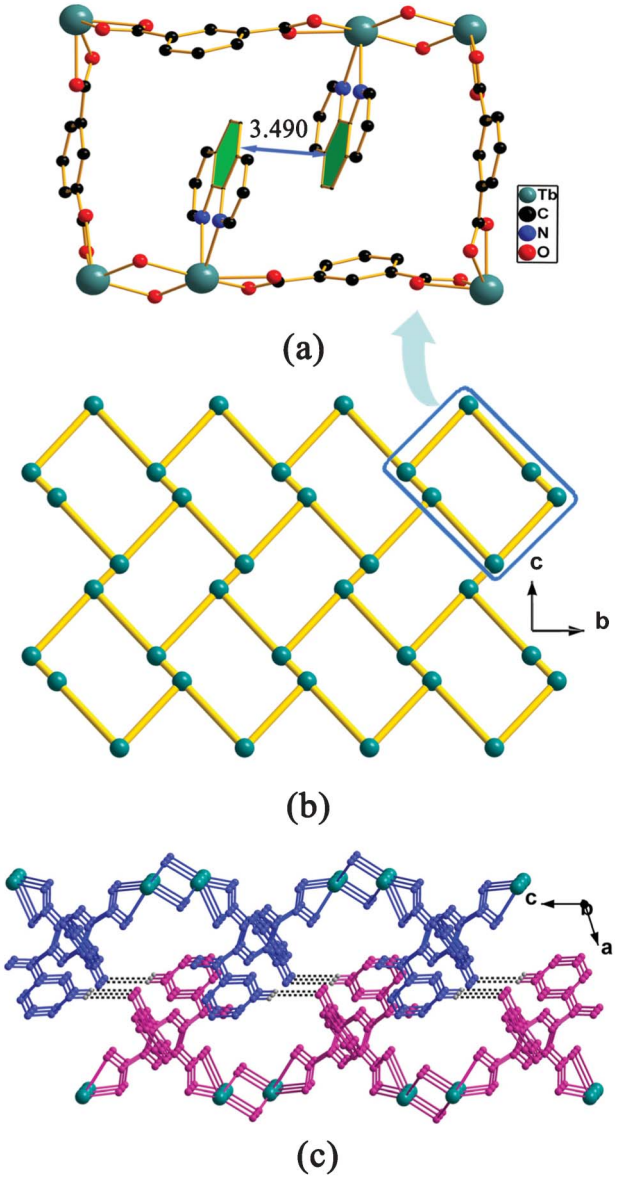

Fig. 3 (a) In **10**, two 1,10-phen ligands fill in the blank of the parallelogram unit (the benzoyl groups and H atoms are omitted for clarity). (b) The 6^3 topological network of **10**. (c) The 3D supramolecular framework constructed *via* the interlayer C21–H21···O3 hydrogen bonds (high-lighting the 2D layers with different colours, and sectional H atoms are omitted for clarity).

ligands, and two coordination water molecules (O1W, O2W), showing a distorted bicapped trigonal prism coordination environment (Fig. 4b). The Ho–O bond lengths range from 2.250(4) to 2.454(4) Å with the mean length of 2.3647 Å, which are comparable to those reported for other Ho(III) complexes.[34] Two adjacent Ho(III) ions are bridged by four carboxyl groups, with two L^1 ligands adopting a *syn–syn* bidentate coordination fashion and two L^2 ligands a *syn–anti* bidentate fashion, affording an irregular paddle-wheel-like $Ho_2O_2(CO_2)_6$ subunit with the Ho···Ho distance of 4.190 Å. As shown in Fig. 4c, the L^2 ligands display a μ_3-(η^1:η^1)-(η^1:η^1) (**e**) mode (Scheme 1e). The L^2 ligands bridge the binuclear lanthanide building blocks into a 1D double-stranded loop-like chain along the *b* axis. The double-stranded loop-like chains are linked by the mode **c** of the L^1 ligands into a 2D layer structure (Fig. 4d) and further linked into a 3D supramolecular architecture through C–H···O (C31–H31···O6) and π···π (Cg(3) > Cg(3) Cg(3): C10 > C11 > C12 > C13 > C14 > C15) interactions (Fig. S3, Tables S3 and S5, ESI†).

Luminescence properties

The luminescence spectra of complexes **3**, **4** and **6–11** were investigated in the solid-state at room temperature and exhibit clear characteristic emission spectra of the corresponding Sm(III), Eu(III), Tb(III) and Dy(III) ions as shown in Fig. 5 and Table S6, ESI.† The emission spectra are similar when the complexes contain the same lanthanide ions. Therefore, only the emission spectra of **3**, **4**, **6** and **7** are described in detail.

Under excitation at 340 nm, the spectrum of **3** exhibits four sharp bands at 562, 596, 642 and 703 nm (assignable to the $^4G_{5/2} \rightarrow {}^6H_J$ (J = 5/2, 7/2, 9/2, 11/2) transitions) characteristic of Sm(III) and consistent with literature reports (Fig. 5a).[34,35] The emission spectrum of **4** with an excitation at 350 nm shows, as anticipated, four peaks at 578, 590, 613 and 696 nm, respectively, assignable to the transitions from deactivation of the $^5D_0$ excited state to the corresponding ^7F_J (J = 0, 1, 2, 4), characteristic of a Eu(III) ion (Fig. 5b). The quite weak emission $^5D_0 \rightarrow {}^7F_0$ at 578 nm is attributed to the symmetry-forbidden emission of the Eu(III) ions in the polymer. The moderately strong emission at 590 nm ($^5D_0 \rightarrow {}^7F_1$) is due to the prominent magnetic dipole transition, which is almost unaffected by the coordination environment. In the spectra, it can be seen that the intensity of the $^5D_0 \rightarrow {}^7F_2$ is much stronger than that of the $^5D_0 \rightarrow {}^7F_1$, suggesting that the Eu(III) ions are located in lower symmetric coordination environments. Additionally, the emission peaks in the $^5D_0 \rightarrow {}^7F_2$ transition region generate the splitting of energy, which can be also ascribed to the Eu(III) centers in asymmetric sites in the complexes. Among these emission lines, the $^5D_0 \rightarrow {}^7F_2$ transitions are the most striking, giving the intense red luminescence of **4**.[17,36] The spectrum of **6** excited at 290 nm (Fig. 5c) exhibits the emission bands characteristic of a Tb(III) ion. The most intense emission at 545 nm corresponds to the hypersensitive $^5D_4 \rightarrow {}^7F_5$ transition, while three moderately strong bands at approximately 488, 586 and 622 nm are assignable to the $^5D_4 \rightarrow {}^7F_6$, $^5D_4 \rightarrow {}^7F_4$ and $^5D_4 \rightarrow {}^7F_3$ transitions, respectively. The weak emissions at 652, 668, and 680 nm are attributable to the transitions of $^5D_4 \rightarrow {}^7F_J$ (J = 2, 1, 0). Complex **6** gives off the vivid green emission characteristic of Tb(III) complexes.[36,37] As shown in Fig. 5d, the spectrum of **7** excited at 290 nm shows characteristic narrow emission bands at 479, 574, 662, 751 nm corresponding to the $^4F_{9/2} \rightarrow {}^6H_J$ (J = 15/2, 13/2, 11/2, 9/2) transitions. The more intensive emission at 574 nm belongs to the transition $^4F_{9/2} \rightarrow {}^6H_{13/2}$ of the Dy(III) ion. The emission at 479 nm is assigned to the transition $^4F_{9/2} \rightarrow {}^6H_{15/2}$, and the weaker emission at 662 nm is attributed to the $^4F_{9/2} \rightarrow {}^6H_{11/2}$ transition in the polymer. Yellow luminescence was observed for complex **7** in the solid-state.[33,34]

The solid-state excitation and emission spectra of the free H_2L^1 and H_2L^2 ligands are at 472 nm (λ_{ex} = 380 nm) and 454 nm (λ_{ex} = 373 nm), respectively (Fig. S4, ESI†). These emission

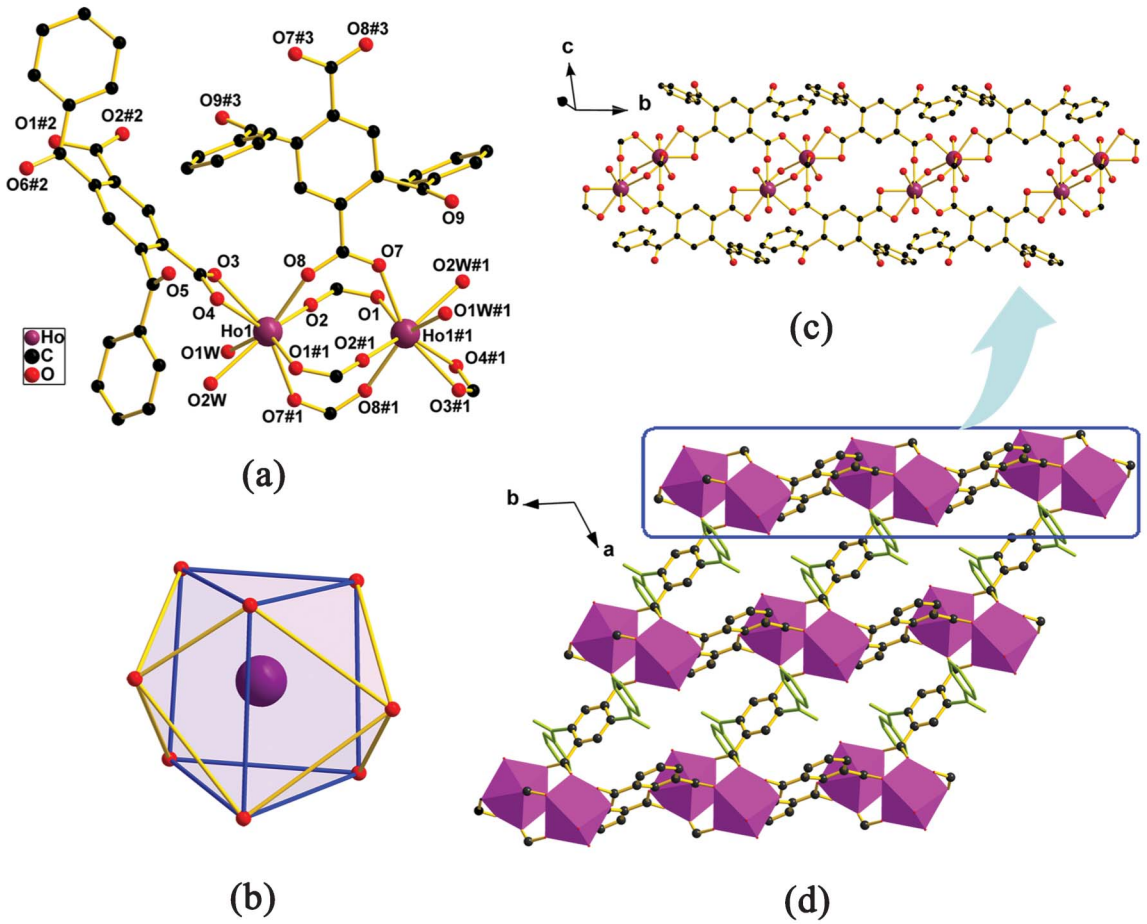

Fig. 4 (a) The coordination environment of Ho(III) in complex **15** (symmetry codes: #1: $-x+1, -y+1, -z+1$; #2: $-x+1, -y+2, -z+1$; #3: $-x+2, -y+2, -z+1$). (b) The distorted bicapped trigonal prism geometry of Ho(III). (c) View the 1D double-stranded loop-like chain along the *b* axis. (d) The 2D parallelogram network. All H atoms are omitted for clarity.

peaks may be assigned to the $\pi^* \rightarrow \pi$ or $\pi^* \rightarrow$ n transitions. The emission peaks of the free H_2L^1 and H_2L^2 ligands are not observed in the corresponding Ln(III) coordination polymers **4** and **6–11**, suggesting efficient energy transfer from the ligands to the Ln(III) ions. In the spectra of **3** (Fig. 5a), it can clearly seen that the baseline is not flat and exhibits a broad band, which may correspond to the emission of the ligand L^1, indicating incomplete energy transfer from the ligands to the Sm(III) ions.[4,38,39] The overall quantum yields, $\Phi_{overall}$, were also determined by means of an integrating sphere and were found to be 0.30% for **3**, 17.20% for **4**, 26.3% for **6**, 0.9% for **7**, 5.3% for **8**, 55.4% for **9**, 40.20% for **10** and 2.00% for **11** under excitation at 340, 350, 290, 290, 290, 290, 365 and 365 nm, respectively. We can find that the overall quantum yields of complexes **8** (Sm(III)), **9** (Eu(III)), **10** (Tb(III)) and **11** (Dy(III)) are higher than those of complexes **3** (Sm(III)), **4** (Eu(III)), **6** (Tb(III)) and **7** (Dy(III)), respectively (Table S6, ESI†). This may be due to the coordination of phen and less O–H oscillators in the coordination sphere in complexes **8–11**.[36,40–42] It is worth mentioning that the overall quantum yield of **3** is much lower than that of **8**, which may be also caused by the incomplete energy transfer from the ligands to the Sm(III) ions in **3**.

The luminescence lifetimes, τ, of the complexes were obtained at room temperature. The f–f electronic transitions of lanthanides are forbidden, leading to a long excited state decay time. The fluorescent decay curves are fitted with a single-exponential function (Fig. S5, ESI†), as a result, the equation $I_t = A_0 + A_1\exp(-t/\tau)$ is utilized for fitting the luminescence decay curves. From Table S6, ESI,† we can find that the lifetime values of **8** (τ = 49.2 μs), **9** (τ = 981 μs), **10** (τ = 762 μs) and **11** (τ = 10.40 μs) are longer than those of **3** (τ = 11.50 μs), **4** (τ = 332 μs), **6** (τ = 675 μs) and **7** (τ = 1.27 μs). These results are consistent with the overall quantum yields results.

IR spectroscopy

In their IR spectra, the strong and broad absorption bands in the range 3300–3600 cm^{-1} are assigned to the characteristic peaks of O–H vibrations of water molecules. Weak bands observed at 3055–3060 cm^{-1} can be attributed to the stretching vibrations of Ar–H. The bands in the range 1655–1670 cm^{-1} and 1394–1405 cm^{-1} indicate the presence of asymmetric and symmetric stretching vibrations of the carboxylate groups, respectively. The absorption bands in the range 1400–1600 cm^{-1} and 690–950 cm^{-1} can be assigned to

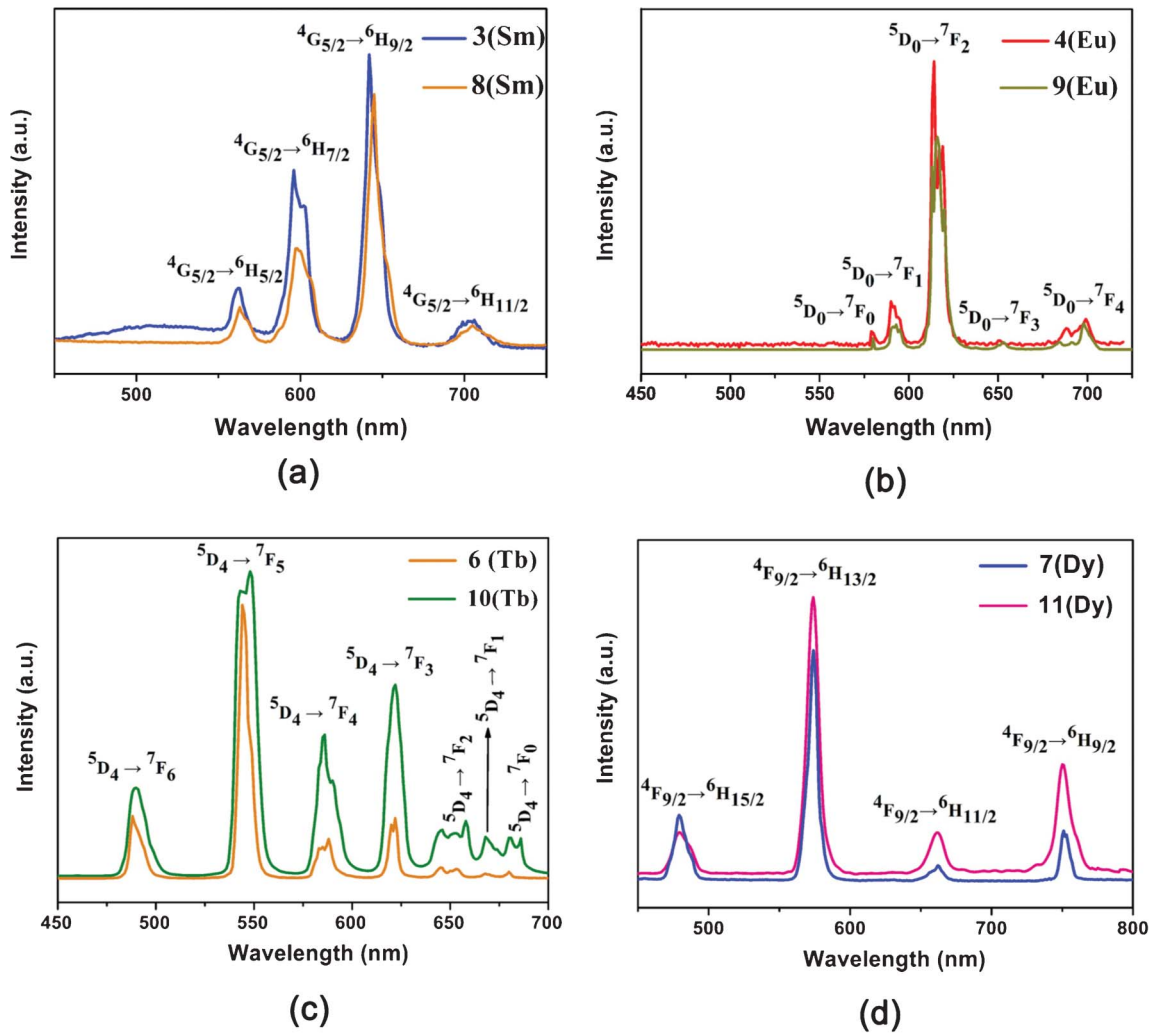

Fig. 5 Solid-state emission spectra of complexes **3** (λ_{ex} = 340 nm), **4** (λ_{ex} = 350 nm), **6** (λ_{ex} = 290 nm), **7** (λ_{ex} = 290 nm), **8** (λ_{ex} = 290 nm), **9** (λ_{ex} = 290 nm), **10** (λ_{ex} = 365 nm) and **11** (λ_{ex} = 365 nm) at room temperature.

the skeletal and bending vibrations of the aromatic ring, respectively.

PXRD and thermal analysis

In order to check the phase purity of these complexes, the PXRD patterns of **1–15** were checked at room temperature. The peak positions of the measured PXRD patterns are in good agreement with the simulated patterns from the respective single-crystal data for the complexes (Fig. S7–S9, ESI†).

Due to the similar thermal decomposition process for isomorphous frameworks, we took complexes **1**, **3**, **10**, **11**, **14** and **15** as representative examples. Their TGA analyses were carried out from room temperature to 800 °C under a nitrogen atmosphere with a heating rate of 5 °C min^{-1}. As shown in Fig. S10, ESI,† the weight loss of complexes **1** and **3** started at 50 °C and was completed at 170 °C, corresponding to the loss of one lattice and two coordinated water molecules. The weight loss of 7.66% for **1** and 7.48% for **3** are in good agreement with the calculated values (7.17% for **1** and 7.08% for **3**). The anhydrous phases are stable between 170 and 340 °C, followed by the subsequent decomposition of the framework. As shown in Fig. S11, ESI,† the TGA curves of **10** and **11** are nearly similar and stable up to 360 and 335 °C, respectively. The organic groups start to decompose gradually and they exhibit continuous weight loss. As illustrated in Fig. S12, ESI,† the TGA curves of complexes **14–15** exhibit a first step starting at about 100 °C and exhibit a continuous weight loss of 5.38% for **14** and 4.87% for **15** up to 195 °C, in agreement with the simulated values (4.73% for **14** and 4.74% for **15**) corresponding to the release of two coordinated water molecules. No obvious thermally stable stages are observed before the collapse of the framework structures begins.

Conclusions

Fifteen lanthanide coordination polymers based on the benzoyl substituted aromatic dicarboxylate H_2L^1 and H_2L^2 ligands were successfully synthesized under hydrothermal conditions. In complexes **1–7**, the binuclear subunits are

linked by L^1 ligands into 3D architectures. Complexes **8–13** show 2D layer structures containing left- and right-handed helical chains, and the 2D layers are further linked by C–H···O, C–H···π and π···π interactions to form 3D supramolecular architectures. Complexes **14** and **15** display 2D layer structures, which formed through L^2 ligands bridging 1D double-stranded loop-like chains. The 2D layers further afford 3D supramolecular architectures linked by C–H···O hydrogen bonds and π···π interactions. Structure studies reveal that the benzoyl can effectively influence the final structure, for instance, by constructing C/O–H···O hydrogen bonds, C/O–H···π and π···π interactions. Complexes **3**, **4** and **6–11** possess good luminescence properties that are characteristic of the respective lanthanide ions. Therefore, the L^1 and L^2 ligands are effective ''antenna'' ligands for the sensitization of the lanthanide luminescence. The study of luminescence properties reveals that the overall quantum yield and lifetime of complexes **8** (Sm(III)), **9** (Eu(III)), **10** (Tb(III)) and **11** (Dy(III)) are higher than those of complexes **3** (Sm(III)), **4** (Eu(III)), **6** (Tb(III)) and **7** (Dy(III)), respectively. This may be due to the coordination of phen to the lanthanide ions and less O–H oscillators in the coordination sphere in complexes **8–11**. The overall quantum yield of **3** is much lower than that of **8**, which may be also caused by the incomplete energy transfer from the ligands to the Sm(III) ions of **3**. This work thus provides helpful information for the design and construction of highly luminescent Ln-based coordination polymers with potential applications in optical and electro-optical devices as well as time-resolved luminescence assays.

Acknowledgements

This work was supported by the NSF of China (21271038, 21071027), the China High-Tech Development 863 Program (2007AA03Z218) and analysis and testing foundation of Northeast Normal University.

References

1 B. Moulton and M. J. Zaworotko, *Chem. Rev.*, 2001, **101**, 1629–1658.
2 J. An, O. K. Farha, J. T. Hupp, E. Pohl, J. I. Yeh and N. L. Rosi, *Nat. Commun.*, 2012, **3**, 604.
3 Y. Cui, H. Xu, Y. Yue, Z. Guo, J. Yu, Z. Chen, J. Gao, Y. Yang, G. Qian and B. Chen, *J. Am. Chem. Soc.*, 2012, **134**, 3979–3982.
4 S. Petoud, S. M. Cohen, J.-C. G. Bünzli and K. N. Raymond, *J. Am. Chem. Soc.*, 2003, **125**, 13324–13325.
5 Y. Takashima, V. M. Martínez, S. Furukawa, M. Kondo, S. Shimomura, H. Uehara, M. Nakahama, K. Sugimoto and S. Kitagawa, *Nat. Commun.*, 2011, **2**, 168.
6 M. D. Allendorf, C. A. Bauer, R. K. Bhakta and R. J. T. Houk, *Chem. Soc. Rev.*, 2009, **38**, 1330–1352.
7 Y. Cui, Y. Yue, G. Qian and B. Chen, *Chem. Rev.*, 2012, **112**, 1126–1162.
8 M. Kurmoo, *Chem. Soc. Rev.*, 2009, **38**, 1353–1379.
9 D. Maspoch, D. Ruiz-Molina and J. Veciana, *Chem. Soc. Rev.*, 2007, **36**, 770–818.
10 C. Benelli and D. Gatteschi, *Chem. Rev.*, 2002, **102**, 2369–2388.
11 B. F. Wicker, H. Fan, A. K. Hickey, M. G. Crestani, J. Scott, M. Pink and D. J. Mindiola, *J. Am. Chem. Soc.*, 2012, **134**, 20081–20096.
12 R. F. D'Vries, V. A. de la Peña-O'Shea, N. Snejko, M. Iglesias, E. Gutiérrez-Puebla and M. Á. Monge, *Cryst. Growth Des.*, 2012, **12**, 5535–5545.
13 P. Wu, J. Wang, Y. Li, C. He, Z. Xie and C. Duan, *Adv. Funct. Mater.*, 2011, **21**, 2788–2794.
14 J.-C. G. Bunzli and C. Piguet, *Chem. Soc. Rev.*, 2005, **34**, 1048–1077.
15 C. Yang, L.-M. Fu, Y. Wang, J.-P. Zhang, W.-T. Wong, X.-C. Ai, Y.-F. Qiao, B.-S. Zou and L.-L. Gui, *Angew. Chem., Int. Ed.*, 2004, **43**, 5010–5013.
16 S. I. Klink, G. A. Hebbink, L. Grave, P. G. B. Oude Alink, F. C. J. M. van Veggel and M. H. V. Werts, *J. Phys. Chem. A*, 2002, **106**, 3681–3689.
17 L.-F. Wang, L.-C. Kang, W.-W. Zhang, F.-M. Wang, X.-M. Ren and Q.-J. Meng, *Dalton Trans.*, 2011, **40**, 9490–9497.
18 H. He, D. Yuan, H. Ma, D. Sun, G. Zhang and H.-C. Zhou, *Inorg. Chem.*, 2010, **49**, 7605–7607.
19 J. Tao, M.-L. Tong and X.-M. Chen, *J. Chem. Soc., Dalton Trans.*, 2000, 3669–3674.
20 X. Guo, G. Zhu, F. Sun, Z. Li, X. Zhao, X. Li, H. Wang and S. Qiu, *Inorg. Chem.*, 2006, **45**, 2581–2587.
21 X.-P. Yang, R. A. Jones, J. H. Rivers and R. Pen-jen Lai, *Dalton Trans.*, 2007, 3936–3942.
22 X. Gu and D. Xue, *Cryst. Growth Des.*, 2006, **6**, 2551–2557.
23 Y.-L. Wang, Y.-L. Jiang, Q.-Y. Liu, Y.-X. Tan, J.-J. Wei and J. Zhang, *CrystEngComm*, 2011, **13**, 4981–4987.
24 C. A. Black, J. S. n. Costa, W. T. Fu, C. Massera, O. Roubeau, S. J. Teat, G. Aromí, P. Gamez and J. Reedijk, *Inorg. Chem.*, 2009, **48**, 1062–1068.
25 C. M. MacNeill, C. S. Day, A. Marts, A. Lachgar and R. E. Noftle, *Inorg. Chim. Acta*, 2011, **365**, 196–203.
26 B. Chen, Y. Yang, F. Zapata, G. Qian, Y. Luo, J. Zhang and E. B. Lobkovsky, *Inorg. Chem.*, 2006, **45**, 8882–8886.
27 X. Zhao, X.-Y. Yu, T.-L. Chen, Y.-H. Luo, J.-J. Yang and H. Zhang, *Inorg. Chem. Commun.*, 2012, **20**, 247–251.
28 Y. Pang, D. Tian, X.-F. Zhu, Y.-H. Luo, X. Zheng and H. Zhang, *CrystEngComm*, 2011, **13**, 5142–5151.
29 D. Du, Z. Jiang, C. Liu, A. M. Sakho, D. Zhu and L. Xu, *J. Organomet. Chem.*, 2011, **696**, 2549–2558.
30 G. M. Sheldrick, *SHELXS 97, Program for the Refinement of Crystal Structure*, University of Göttingen, Germany, 1997.
31 Z.-P. Deng, L.-H. Huo, H.-Y. Wang, S. Gao and H. Zhao, *CrystEngComm*, 2010, **12**, 1526–1535.
32 P. Chen, H. Chen, P. Yan, Y. Wang and G. Li, *CrystEngComm*, 2011, **13**, 6237–6242.
33 J. Yang, S.-Y. Song, J.-F. Ma, Y.-Y. Liu and Z.-T. Yu, *Cryst. Growth Des.*, 2011, **11**, 5469–5474.
34 Y.-g. Sun, B. Jiang, T.-f. Cui, G. Xiong, P. F. Smet, F. Ding, E.-j. Gao, T.-y. Lv, K. Van den Eeckhout, D. Poelman and F. Verpoort, *Dalton Trans.*, 2011, **40**, 11581–11590.
35 Q.-F. Yang, Y. Yu, T.-Y. Song, J.-H. Yu, X. Zhang, J.-Q. Xu and T.-G. Wang, *CrystEngComm*, 2009, **11**, 1642–1649.
36 M. V. Lucky, S. Sivakumar, M. L. P. Reddy, A. K. Paul and S. Natarajan, *Cryst. Growth Des.*, 2011, **11**, 857–864.

37 S. Sivakumar, M. L. P. Reddy, A. H. Cowley and R. R. Butorac, *Inorg. Chem.*, 2011, **50**, 4882–4891.
38 D.-P. Dong, L. Liu, Z.-G. Sun, C.-Q. Jiao, Z.-M. Liu, C. Li, Y.-Y. Zhu, K. Chen and C.-L. Wang, *Cryst. Growth Des.*, 2011, **11**, 5346–5354.
39 Y.-X. Chi, S.-Y. Niu and J. Jin, *Inorg. Chim. Acta*, 2009, **362**, 3821–3828.
40 Y. Haas and G. Stein, *J. Phys. Chem.*, 1971, **75**, 3677–3681.
41 Y. Li, F.-K. Zheng, X. Liu, W.-Q. Zhou, G.-C. Guo, C.-Z. Lu and J.-S. Huang, *Inorg. Chem.*, 2006, **45**, 6308–6316.
42 P. Lenaerts, K. Driesen, R. Van Deun and K. Binnemans, *Chem. Mater.*, 2005, **17**, 2148–2154.